

Angle-resolved photoemission studies of the valence-band structure of stepped crystal surfaces: Cu(S)-[3(111)×(100)]

R. F. Davis,* R. S. Williams,† S. D. Kevan,‡
P. S. Wehner,§ and D. A. Shirley

Materials and Molecular Research Division, Lawrence Berkeley Laboratory, Berkeley, California 94720
and Department of Chemistry, University of California, Berkeley, California 94720

(Received 13 September 1984)

Angle-resolved photoemission spectra are reported for the stepped Cu(211) face in the photon-energy range $9 \leq h\nu \leq 34$ eV. The valence-band (VB) spectra are interpreted in terms of a direct-transition model for bulk photoemission. Determination of VB dispersion relations and assignment of the bands are aided by use of selection rules involving the transmitted-radiation vector potential and several different experimental geometries. The major results are (1) it is possible to determine experimental VB dispersion relations for a lower-symmetry direction such as Cu[211], and (2) VB dispersion relations for stepped Cu(211) show excellent agreement with bulk valence bands interpolated along the [211] direction, uninterrupted by band-gap photoemission, the effects of which are not observed. It is concluded that the unusual structure of the stepped surface does not significantly perturb the bulk electronic structure near the surface in this case.

I. INTRODUCTION

Detailed angle-resolved-photoemission (ARP) studies of the face-centered-cubic (fcc) metals copper,¹⁻⁵ silver,^{6,7} gold,⁸⁻¹¹ nickel,¹² palladium,¹³ platinum,^{8,14} and iridium¹⁵ have shown that the peak structures in photoelectron energy-distribution curves (EDC's) arise mainly from energy- and crystal-momentum-conserving direct electronic transitions near or at the surface. Consequently, by combining the photon-energy variability of synchrotron radiation with a normal electron-emission geometry, these studies^{1,2,4,6,8,9,12-15} have resulted in the determination of empirical bulk valence-band dispersion relations along \vec{k}_\perp (the surface perpendicular or normal component of the crystal momentum \vec{k}) with remarkable success. However, in each case, the surface studied was a low-Miller-index plane [i.e., (100), (110), or (111)]. These studies yielded experimental energy bands along high-symmetry lines in \vec{k} space, permitting ready comparisons to published theoretical band-structure calculations.

In this paper we report angle-resolved normal-photoemission (ARNP) valence-band studies of the Cu(211) face, a Cu(S)-[3(111)×(100)] stepped surface, of which an ideal segment is depicted in Fig. 1. These experiments address *directly* a number of important problems in photoemission from metals. The complexity of ARNP from (110) and (100) faces¹⁶ relative to (111) suggests that a detailed understanding of ARNP from still lower-symmetry faces—such as (211)—might be very difficult. This hypothesis has several origins. First, low k -space symmetry completely lifts the degeneracy of the energy bands along much of the [211] line. Second, the relatively large surface unit cell of a high-index face gives rise to a set of small two-dimensional reciprocal-lattice vectors which may induce surface umklapp of photoelectrons with a cross section higher than that on unreconstructed

low-index faces.¹⁷ Furthermore, like many high-index faces of the group-VIII and -IB metals oriented in the [01 $\bar{1}$] crystallographic zone,¹⁸ the clean Cu(211) surface develops a stable stepped structure after annealing. The electronic structure of stepped and kinked surfaces is of considerable interest because the step and/or kink atoms on such surfaces are believed to influence surface reactivity.¹⁹ Although there is some experimental²⁰ and theoretical²¹ evidence that enhancement of surface reactivity may arise more from steric effects due to step-adsorbate geometry than from any particular electronic-structural property of the steps, some theoretical calculations predict, in certain cases, substantially different electronic environments for step or kink atoms relative to atoms on planar surfaces.^{22,23}

A detailed understanding of the photoemission process from Cu(211) is obtained simply within the framework of the direct-transition model using a quasi-free-electron

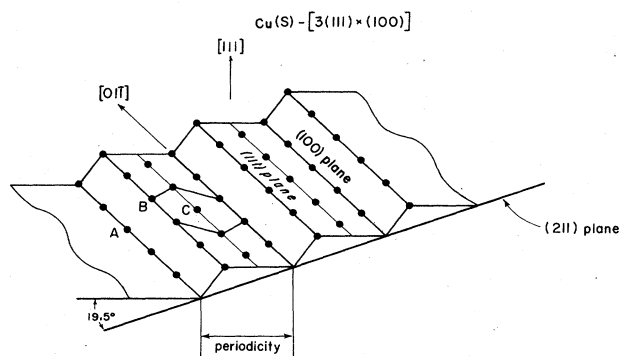


FIG. 1. Segment of an ideal Cu(S)-[3(111)×(100)] surface, showing three-atom terraces of (111) orientation separated by monatomic steps of (100) orientation. The (01 $\bar{1}$) mirror plane intersects the surface perpendicular to the atomic rows.

final-state band structure. Furthermore, although the low symmetry of Cu(211) does indeed introduce a great deal of the structure of the EDC's, it also enables us to investigate the symmetry and dispersion properties of each individual valence band.

In Sec. II we discuss experimental procedures. In Sec. III we describe the results within a bulk direct-transition framework, and in Sec. IV we summarize our study.

II. EXPERIMENTAL PROCEDURE

A high-purity single-crystal slab of Cu was cut and mechanically polished to within $\pm 0.5^\circ$ of the (211) plane (19.5° from [111] in the $[01\bar{1}]$ zone), with a mean surface roughness of $1\ \mu\text{m}$. After a chemical polish,²⁴ the crystal was installed in an ultrahigh-vacuum chamber (base pressure $\sim 3 \times 10^{10}$ Torr) for *in situ* preparation and characterization.^{18,25} Preparation was accomplished by repeated cycles of Ar^+ -ion sputtering, followed by annealing at ~ 875 K. Immediately preceding the ARP experiments, the resulting surface was monitored by Auger-electron spectroscopy (AES) for cleanliness and low-energy electron diffraction (LEED) for crystallographic order, giving rise to AES impurity signals characteristic of ≤ 0.05 monolayer contamination and LEED patterns (with extremely sharp and intense spots) characteristic of the stable step-surface structure. As shown in Fig. 1, the (211) surface consists of (111)-oriented terraces with three inequivalent atomic rows (labeled *A*, *B*, and *C*) that are parallel to the $[01\bar{1}]$ direction, and monatomic steps of (100) orientation. The only symmetry element that this surface contains is the $(01\bar{1})$ mirror plane, which intersects the surface perpendicular to the atomic rows.

The photoemission measurements were performed on the 8th branch of beam line I (BL I-2) at the Stanford Synchrotron Radiation Laboratory (SSRL). The incident radiation was highly polarized ($> 97\%$) in the horizontal plane and in the energy range $9 \leq h\nu \leq 34$ eV. Our ARP instrument, described elsewhere,²⁶ employs a rotatable 5.40-cm-mean-radius hemispherical analyzer with an angular acceptance of $\pm 3^\circ$. In these measurements the energy resolution (monochromator plus electron analyzer) varied from about 0.12 to about 0.25 eV [full width at half maximum (FWHM)] at the lower and upper photon energies, respectively.

As shown in Fig. 2, experiments were done with two different normal-emission geometries, conversion between which was achieved by azimuthal rotation of the crystal about its normal (\vec{n}) by 90° . For both orientations, the incident-radiation vector potential (\vec{A}) was confined to the plane of incidence, and the photoemission direction (\vec{p}) was confined to the surface normal ($[211]$). In orientation I [Fig. 2(a)], \vec{A} lies in a crystallographic plane perpendicular to the $(01\bar{1})$ mirror plane (*M*) with $\phi_A = 0^\circ$, whereas in orientation II [Fig. 2(b)], \vec{A} lies in *M* (*M* is the plane of incidence in this case) with $\phi_A = 270^\circ$. The angle θ_A (between \vec{n} and \vec{A}) could be varied between 10° and 45° in either θ_A azimuth by coupling analyzer and crystal polar rotations, but the majority of measurements were performed with $\theta_A = 30^\circ$. At this angle, \vec{A} is aligned with the $[110]$ direction in orientation I, and is $\sim 5^\circ$ from align-

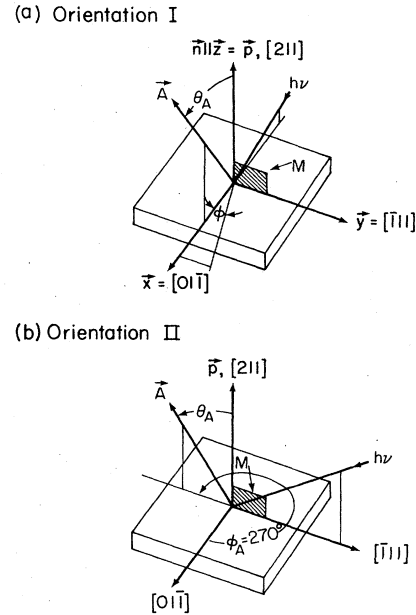


FIG. 2. Experimental geometries employed: (a) orientation I, with the plane of incidence perpendicular to the $(01\bar{1})$ mirror plane *M*; (b) orientation II, with the plane of incidence parallel to *M*. The majority of spectra were recorded with θ_A , the angle between the surface normal \vec{n} and the incident-radiation vector potential \vec{A} , equal to 30° .

ment with $[100]$ in orientation II. *In situ* polar crystallographic alignment ($\pm 1^\circ$) was achieved using a He-Ne laser, and the azimuthal orientation ($\pm 3^\circ$) was determined from LEED patterns. We shall henceforth refer to the above sample orientations simply as I and II.

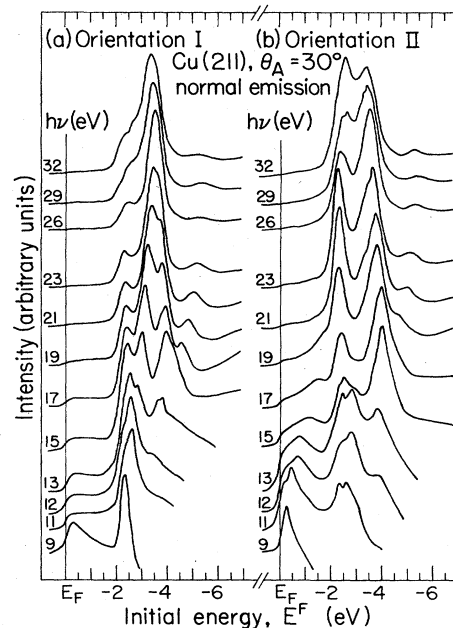


FIG. 3. Selected normal photoemission spectra for Cu(211) with photon energies in the range $9 \leq h\nu \leq 32$ eV and $\theta_A = 30^\circ$. The spectra in panel (a) were collected with the orientation I geometry, while those in (b) were recorded with orientation II.

Typical EDC's for the entire energy range are shown in Fig. 3 for both orientations and $\theta_A=30^\circ$. For brevity, only 24 spectra are plotted here. Our interpretation is based on a total of 82 spectra. In each spectrum, the Fermi level (E_F) was determined as $(dI/dE)_{\max}$, i.e., the point of the maximum derivative of photoelectron intensity with respect to energy, in the region near the onset of the s - p plateau. Because of relatively low intensity (I), this procedure became progressively more difficult in the higher-photon-energy region ($h\nu \geq 20$ eV), particularly for the spectra taken with the sample in orientation I. Nevertheless, the work functions derived from E_F placement and analyzer reference voltages showed an rms scatter of only ± 35 meV for the entire data set.

III. RESULTS AND DISCUSSION

The spectra shown in Fig. 3 clearly indicate that (a) the low symmetry of the (211) face introduces complexity to the valence-band peak structure relative to the spectra of low-index Cu faces, and (b) there is a strong dependence on radiation polarization, as the only difference between the two orientations is the direction of \vec{A} relative to the crystallographic axes. The behavior of the various contributions to the spectra, which can be identified and shown to disperse with photon energy, is highly indicative of bulk direct-transition processes, particularly because \vec{k}_{\parallel} (surface component of momentum) is zero for normal emission. This behavior is demonstrated by the structure plots for both orientations, shown in Fig. 4. The circles represent strong peak (solid circles) or weak feature (open

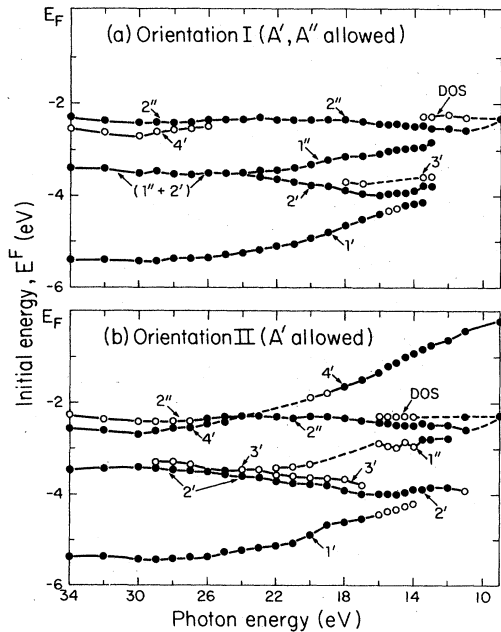


FIG. 4. Plot of experimental peak position vs photon energy for each structure in the Cu(211) EDC's for $\theta_A=30^\circ$: (a) orientation I; (b) orientation II. Open and solid circles designate weak and strong features, respectively, and the connecting lines have no theoretical significance. The plots are labeled with the appropriate initial states involved in direct transitions.

circles) energy positions relative to E_F or the range of photon energies used. The connecting lines on the plots in Fig. 4 have no significance other than to join and map the individual structures as a function of $h\nu$. The reproducibility between the two sets of plots (orientations I and II) is excellent: The derived energies of equivalent peaks which are found in spectra for both orientations (at a given $h\nu$) typically agree within 0.04 eV or less. The bands are labeled according to a notation to be described below.

In the normal-emission geometry, peak energy dispersion with $h\nu$ as shown in Fig. 4 can only occur from direct transitions at reduced \vec{k} points that yield photocurrent in normal emission, i.e., \vec{k} points that either are part of the [211]-direction crystal-momentum space (primary Mahan cones²⁷), or are in other directions but can excite transitions that result in normal emission via surface umklapp processes (secondary cones^{17,28}). Below, we proceed to set up a bulk band-structure framework²⁹ with which to interpret the data represented in Figs. 3 and 4, and we show that excellent agreement between experiment and theory is obtained if (a) only \vec{k}_{\perp} -conserving transitions from [211] initial states are assumed to occur, and (b) only one final-state band is important in transmitting photocurrent to the analyzer (i.e., no secondary Mahan cones contribute *peak* structures).

The irreducible portion of \vec{k} space lying along [211], all of which is contained in the $(01\bar{1})$ plane, is shown as the dashed line in Fig. 5. The point $B=(\frac{3}{4}, \frac{3}{8}, \frac{3}{8})$ (in units of $2\pi/a$, which will be used throughout this work) is equivalent to $D=(-\frac{1}{4}, -\frac{5}{8}, -\frac{5}{8})$, both being at the Brillouin-zone boundary. Although these points have no other significance or special symmetry properties, it is useful to designate them B and D . The group of the \vec{k} vector (the point group C_2) corresponding to points along [211] ($\Gamma \rightarrow B, D \rightarrow X$) contains only the identity element (E) and the $(01\bar{1})$ mirror plane (σ_h). Thus, electronic states lying on the [211] crystal-momentum axis may be symmetry-classified as either even or odd (A' or A'' ,

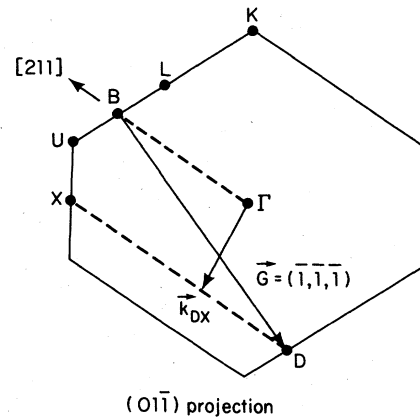


FIG. 5. $(01\bar{1})$ mirror plane, showing the region of k space in the first Brillouin zone along the [211] direction (dashed lines). The points B and D , both at the zone boundary, are separated by an umklapp with $\vec{G}=(2\pi/a)(\bar{1}, \bar{1}, \bar{1})$. The vector \vec{k}_{DX} , ending at a general point along the $D-X$ line, is thus not actually in the [211] direction in the reduced-zone scheme.

respectively, in C_s) with respect to reflection through the mirror plane.

The energy bands for Cu were generated for the [211] crystal-momentum line using Smith's band-structure interpolation scheme, which utilizes a mixed basis set consisting of five atomic d orbitals and 16 plane waves,³⁰ and is an extension of the Hodges-Ehrenreich-Lang formalism.³¹ The parameters used for the calculation were obtained in Ref. 30 by fitting to the energy bands of Janak *et al.*,³² stretching the valence band by 8% along the energy scale to agree with photoemission data. The agreement of the interpolated bands with the first-principles results of Janak *et al.*³² and with those of Burdick³³ are quite good, even extending 20 eV above the Fermi level. The energy bands were generated along the [211] direction by folding the dashed lines shown in Fig. 5 into the irreducible $\frac{1}{48}$ th wedge of the first Brillouin zone with $k_y \geq k_x \geq k_z \geq 0$, and diagonalizing the interpolation Hamiltonian for the resulting \vec{k} values.

From careful inspection of the eigenvectors in our calculation, we determined the irreducible representations (A' or A'') of the first eight bands at each \vec{k} point, and labeled the bands shown in Fig. 6 accordingly. We found it useful to label the bands of each type separately according to increasing band index, but this has no group-theoretical significance. It does, however, remove ambiguities caused by band crossings. Of the six valence bands, four have A' symmetry, while the two lowest conduction bands also have A' symmetry. As shown, the band structure reveals a gap in the conduction bands between A'_5 and A'_6 from about 10.8 to 12.0 eV above E_F , and a rather complex behavior beginning at 23.7 eV above E_F . In principle, a conduction-band gap has implications for ARP if it involves the photoemission final states.^{17,28,34}

Hermanson³⁵ has discussed the polarization-selection rules for photoemission normal to low-index faces of cubic crystals, and there have been several experimental studies of these polarization effects.^{2,36} In this study we have incorporated two different polarization geometries to investigate the importance of these effects for a stepped crystal face, for which the symmetry properties are simple. Polarization selection actually reduces considerably the problem of determining dispersion relations for each individual valence band in Cu(211), as will be discussed below. The selection rules governing ARNP from Cu(211) are summarized in Table I. The photoemission final state must belong to the A' (symmetric) irreducible representation because operations which leave the crystal

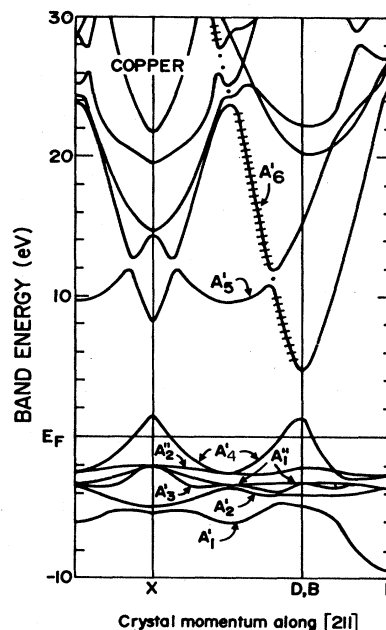


FIG. 6. Band structure of Cu interpolated along the [211] direction. The energy bands are symmetric about X , and the unoccupied bands are shown up to $E^F=30$ eV. The bands are labeled by A' and A'' irreducible representations. The A' -symmetry final-state bands that carry photocurrent in the [211] direction are highlighted by cross hatches, with solid dots used to bridge the band-gap regions.

invariant should not affect the electronic state sampled by the detector. Thus, in order for a transition to be allowed, the irreducible representation of a particular initial state must be contained in the transition operator $\vec{A} \cdot \vec{p}$. Referring to Fig. 2 and Table I, the component of \vec{A} along [011] (orthogonal to M) can excite A'' initial states (A''_1 or A''_2), while components along [211] and $[\bar{1}11]$ (lying in M) excite only A' (A'_1 through A'_4) initial states. Thus, for the geometries shown in Fig. 2, the spectra accumulated in orientation I may arise from $A' \rightarrow A'$ and $A'' \rightarrow A'$ transitions. On the other hand, the spectra from orientation II, with $A_x=0$, should arise from A' initial-state bands only. Inspection of relative peak intensities in the spectra (Fig. 3) indicates a qualitative verification of these selection rules for Cu(211) direct transitions. Aided by direct comparison of interpolated and experimental band structures (see below), we have labeled the structure plots in Fig. 4 according to the initial states involved in the transitions.

TABLE I. Polarization-selection rules for normal photoemission from (211) faces of fcc crystals. The photoelectron propagation direction defines the z axis in each case.

Coordinate axes			Irreducible representations	Final-state symmetry	Allowed initial-state symmetries		
x	y	z			A_x	A_y	A_z
[01 $\bar{1}$]	$[\bar{1}11]$	[211]	A', A''^a	A'	A''	A'	A'

^aSince the [211] axis in momentum space has no special symmetry designation, the symbols A' and A'' chosen to represent the even and odd states, respectively, are those for the usual C_s -symmetry classification.

In agreement with previous studies,^{6,8,9,14} the photoemission final states were taken partly to be A' conduction-band components that are derived from the empty-lattice conduction band(s) that would be involved in [211] primary Mahan²⁷ cone emission. Between Γ and B , there are no unbound primary-cone components for photoemission with $h\nu \leq 34$ eV, since the smallest reciprocal-lattice vector involved in a primary-cone transition $\vec{k}_i \rightarrow \vec{k}_i - \vec{G}$ (in the empty-lattice approximation) would be $\vec{G} = (4, 2, 2)$; this would require $h\nu > 170$ eV at $\vec{k}_i = B$. However, there is primary emission in our energy range from final states between D and X , shown in Fig. 6 as the regions of A'_5 and A'_6 highlighted by cross hatches. These states are derived from $\vec{G} = (\bar{1}, \bar{1}, \bar{1})$. In the band-gap regions, $10.8 \leq E^F \leq 12.0$ eV and $E^F \geq 23.7$ eV, the final states were derived from

$$E^F(\vec{k}) = (\hbar^2/2m^*) |\vec{k} - \vec{G}|^2 + V_0^F,$$

with $\vec{G} = (\bar{1}, \bar{1}, \bar{1})$. These states are shown in Fig. 6 as solid circles between A'_5 and A'_6 and extending beyond A'_6 . The parameters m^* (reduced mass) and V_0^F (inner potential) were calculated from a fit of this free-electron-like dispersion relation to the regions of A'_5 and A'_6 , highlighted by cross hatches in Fig. 6, yielding $m^* = 0.89m_e$ and $V_0^F = -8.0$ eV. This value of m^* is consistent with that determined experimentally by Knapp *et al.*² for the Δ_1 conduction band in Cu(001) ($m^*/m_e = 0.90-0.94$). Using the measured³⁷ value for the Cu(211) work function ($\Phi = 4.53$ eV), we obtain $V_0^v = -12.5$ eV (V_0^v is the vacuum-referenced inner potential) for our final-state band, reasonably consistent with the value determined from LEED studies³⁸ of Cu(001) ($V_0^v = -13.5$ eV). In contrast to several previous studies (see, e.g., Ref. 14), this Cu(211) quasi-free-electron final-state dispersion relation was used without modification.

In Fig. 7 we show a comparison of our empirically derived valence-band positions (symbols) with the interpolated dispersion relations (lines) for all six valence bands along [211]. The arrows at E_F indicate \vec{k} values for which A'_4 intersects the Fermi surface (from de Haas-van Alphen data³⁹). The empirical bands in Fig. 7 represent the combined data of orientations I and II (Figs. 3 and 4). If a peak appeared in both orientations, the mean value was used to determine the band position. The points in Fig. 7 were positioned in the standard way²⁹ by determining \vec{k}_i from the final-state band highlighted in

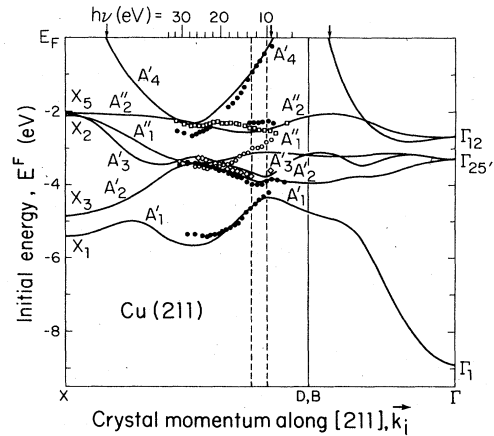


FIG. 7. Empirical [symbols: \bullet — A'_1 , A'_2 , A'_4 , and DOS; \diamond — A'_3 ; \circ — A'_1 ; and \square — A'_2] and theoretical (solid lines, from interpolated bands in Fig. 6) valence-band dispersion relations for Cu(211). A partial photon-energy scale is indicated at E_F , and the vertical arrows are from de Haas-van Alphen data (Ref. 39). The dashed vertical lines bracket the region for which the \vec{k} vectors lie in the bulk conduction-band gap.

Fig. 6. Then, for each valence band, the points were fitted to a smooth curve, yielding empirical dispersion relations.

Considering both the complexity of the Cu(211) EDC's and the possible inaccuracies associated with the interpolation-scheme calculation,³¹ the theoretical and experimental bands generally agree quite well and both agree with the Fermi-surface data.³⁹ The only feature in the EDC's that does not appear to arise from direct transitions is a weak shoulder at $E^F = -2.30 \pm 0.02$ eV in the spectra for $9 \leq h\nu \leq 16$ eV. It is reasonable to attribute this nondispersing feature to the d -band edge in the density of states. A similar feature was noted in silver,⁶ gold,⁸ and platinum⁸ ARNP spectra.

We can describe the "agreement" between experiment and interpolation theory quantitatively by calculating $\Delta E = E^F(\text{expt}) - E^F(\text{int})$ for each energy level determined in this investigation, where $E^F(\text{int})$ is the interpolated energy position. The results are listed in Table II, along with similar (theoretical) numbers reported by Hodges *et al.*³¹ for a general comparison of interpolated Cu bands with Burdick's³³ APW calculation. The theoretical ΔE

TABLE II. Deviations between experimental and theoretical valence bands along the [211] direction in copper.

Deviation parameter	Magnitude for valence bands along [211] (eV)						Overall theoretical ΔE^b
	A'_1	A'_2	A'_3	A'_1	A'_2	A'_4	
$[\Delta E]_{\text{av}}$	0.11	0.04	0.06	0.01	0.06	0.20	0.09
ΔE_{rms}^c	0.10	0.05	0.06	0.11	0.10	0.14	0.11
$ \Delta E _{\text{max}}^d$	0.29	0.10	0.11	0.24	0.21	0.32	0.37

^a $\Delta E_i = E^F(\text{expt}) - E^F(\text{int})$.

^bFrom comparison of interpolation scheme with Burdick's bands (Ref. 33) in copper, at 89 \vec{k}_i points in the Brillouin zone; taken from Ref. 31.

^c ΔE_{rms} denotes root-mean-square deviation.

^d $|\Delta E|_{\text{max}}$ denotes maximum deviation.

values represent the general limitations of the interpolation method and thus are lower bounds on the size of ΔE values that might reasonably be expected for these Cu(211) studies. Conversely, experimentally derived ΔE values that are smaller than those of Hodges *et al.*³¹ are not meaningful. By this criterion, the differences between the interpolated and experimental band structures are negligible for all bands except A'_1 and A'_4 . However, there are no gross deviations of the experimentally determined bands from those generated by the interpolation procedure, and the deviations that do occur may very well be caused by the finite resolution of the electron-energy analyzer coupled with the inability to separate overlapping spectral features properly. In general, the agreement between the experimental and interpolated bands is quite good, and this represents the most significant result of this work.

The components of the vector potential \vec{A} that are parallel to M (A_z, A_y) can excite A' transitions and A_x (perpendicular to M) excites A'' transitions, if the polarization-selection rules are obeyed in Cu(211) (see Table I). Figure 8 illustrates the effect of polarization-selection rules on Cu(211) ARNP spectra, for selected photon energies. The intensities vary as expected. Finite angular acceptance of the analyzer ($\pm 3^\circ$), angular alignment ($\pm 1^\circ$ in θ , $\pm 3^\circ$ in ϕ), and incomplete polarization of the radiation ($> 97\%$ polarized) are among the effects that contribute to the apparent violation of these rules, which takes the forms of weak photoemission from A'_1 and somewhat stronger emission from A'_2 in orientation II, where they are both forbidden because $|A_x| = 0$ (see Fig. 2). In orientation I, where both $|A_x|$ and $|A_z|$ are nonzero, there is no A'_4 peak except at higher photon energies, and A'_1 typically dominates over A'_2 and A'_3 . In order to understand in detail these intensity variations,

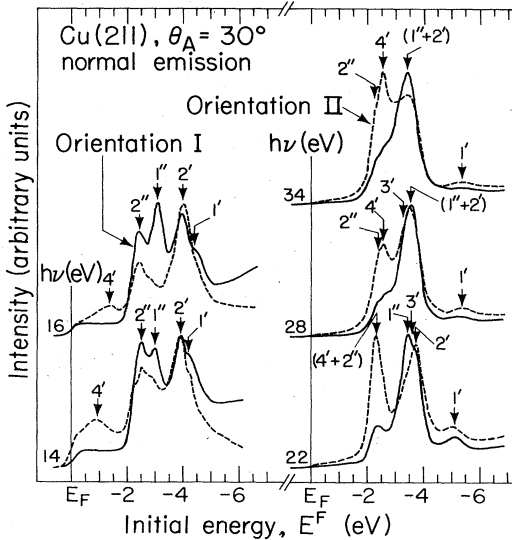


FIG. 8. Direct comparison of photoemission spectra at selected photon energies for both orientations, with $\theta_A = 30^\circ$, showing a strong dependence on radiation-polarization orientation. The structures are labeled by the appropriate bands involved in direct transitions.

one must know the electromagnetic field as it passes through the vacuum-solid interface⁴⁰ and the transition matrix elements. Smith *et al.*⁴¹ have discussed these effects in the ARP polarization studies of Cu(111) by Knapp *et al.*²

It is interesting to compare EDC's for different θ_A . In Fig. 9, spectra at $h\nu = 17$ eV are shown for both orientations (I and II) and $\theta_A = 10^\circ, 30^\circ$, and 40° , corresponding to different electric field strengths normal and parallel to the sample surface. For orientation II, the spectra are normalized to the intensity of $A'_2 + A'_3$ (this is essentially A'_2 at this energy), and orientation I EDC's are normalized to the A'_1 intensity. Generally, only changes in relative peak intensities are induced by varying θ_A at all photon energies studied. New peak structures are *not* observed. In orientation II, $|A_x| = 0$; thus, the relative intensities of the four A' peaks in orientation II ($A'_4, A'_3 + A'_2$, and A'_1) do not change significantly with θ_A . However, it was noted above that residual experimental misalignment effectively leads to $|A_x| \geq 0$. Therefore, decreasing θ_A in orientation II suppresses the residual $|A_x|$ component in a manner similar to orientation I, accounting for the observed attenuation of A'_2 intensity in orientation II.

Previous experimental and theoretical work on low-index faces^{17,28,34} showed evidence for unusual behavior in ARP when the excitation energy placed photoelectrons into bulk conduction-band gaps. The main feature supporting this is a "lack of dispersion" of the initial-state bands,³⁴ arising because the \vec{k} vector of the photoelectron is imaginary in the gap, thereby allowing only states at the surface to be excited.^{17,28} Because $|\vec{k}_\parallel| = 0$ in normal emission, band-gap photoemission corresponds to pho-

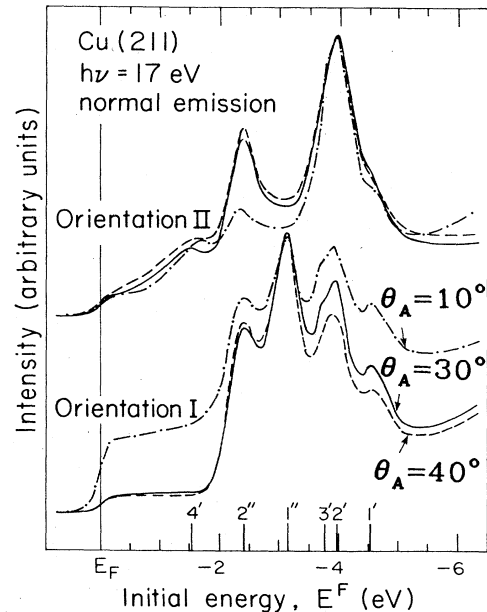


FIG. 9. Direct comparison of photoemission spectra at $h\nu = 17$ eV and various values of θ_A for both orientations. The direct-transition peak positions are indicated on the horizontal axis.

toexcitation from $\bar{\Gamma}$, independent of photon energy. Hence, sweeping the photon energy resulted in direct transitions with concomitant valence-band dispersion as \bar{k}_1 was varied across the zone, until the gap was reached.³⁴ However, bulk conduction-band gaps along high-symmetry directions invariably occur at Γ and/or zone boundaries, and it could be argued equally well that the lack of dispersion is simply a consequence of $v_g \sim 0$ for the initial-state bands. Additionally, lack of dispersion in d bands is not necessarily indicative of band-gap photoemission because they are already reasonably flat.

As a consequence of low symmetry, the conduction-band gap between A'_5 and A'_6 in Cu[211] occurs away from the zone boundary, where initial-state s and sp bands (A'_1 and A'_4 , respectively) have large group velocities. The experimental dispersion relations in Fig. 7 show that there is no evidence for the band-gap photoemission process discussed previously. The portion of the band structure expected to be affected by the bulk band gap is enclosed within the vertical dashed lines. The s and sp bands disperse throughout the gap region, and the absolute sp -band and d -band intensities show no unusual structure in the spectra for either orientation. Previous work in this laboratory on low-index faces of Ag (Ref. 6), Au (Refs. 8 and 9), and Pt (Refs. 8 and 14) also showed initial-state dispersion at photon energies for which the final states should be in a conduction-band gap, but the present Cu(211) work is by far the most convincing evidence for this, because of the large slope in the A'_1 and A'_4 bands away from the zone boundary. Furthermore, Fig. 7 shows that d -band dispersion in the gap region is minimal in both theory (interpolated bands) and experiment, indicating that a dispersionless d band is not sufficient evidence for a band-gap photoemission process.

The apparent lack of band-gap photoemission leads directly to a discussion of the final-state band structure in ARP and the success of the single-plane-wave approximation for its dispersion relation. It has been shown that the finite lifetime of the photoelectron (which is relatively short in Cu at these energies²) introduces an imaginary component to its \bar{k} vector regardless of its position in the zone,⁴² and that the effect of this momentum broadening is essentially to bridge the gaps in the band structure, giving rise to more free-electron-like conduction bands.^{42,43} Damping attenuates the interaction between the photoelectrons and the periodic lattice potential,⁴³ and, since band gaps arise essentially from Bragg scattering, it is not surprising that damping closes these gaps. Strictly speaking, all of this points to the inadequacy of the one-electron band-structure model in describing photoelectron dispersion relations.⁴⁴

IV. SUMMARY AND CONCLUSIONS

We have presented results of normal-emission ARP studies using variable-energy synchrotron radiation for the stepped Cu(211) face. The photoemission process is similar to low-Miller-index faces of copper.^{1,2,4} All peak structures in the EDC's, except for a previously observed density-of-states (DOS) feature at the leading edge of the $3d$ bands and the s - p plateau, are shown to derive from

nearly- \bar{k} -conserving direct transitions along the [211] direction in \bar{k} space. The presence of the stepped surface does not introduce any other spectral features, although part of the photoemission intensity in various peaks (particularly A'_2 in orientation II) may arise from DOS photoemission. Excellent agreement between peak-energy positions and bulk initial-state dispersion relations is obtained if the final-state wave function is assumed to contain only one plane-wave component, i.e., no secondary Mahan emission features were found. This agreement with the interpolated bulk bands suggests that any photoelectron refraction effects associated with non-normal emission, i.e., from step and/or terrace directions, are negligible in this case. In agreement with previous work,^{5,29} a quasi-free-electron parabolic final-state dispersion relation was used successfully, even at energies corresponding to symmetry band gaps near the zone boundary. The top and bottom valence bands, A'_4 and A'_1 , are shown to disperse even when the final state falls in these gap regions, suggesting that the one-electron bulk band-gap picture is not applicable to the description of photoelectron conduction-band structure. Finally, radiation-polarization-selection rules are observed to play an important role in determining relative peak intensities. This is demonstrated in a particularly straightforward manner with Cu(211) because there are only two irreducible representations (A' and A'') for eigenstates along the [211] direction. In fact, polarization selection greatly reduces the problem of determining individual band empirical dispersion relations along the complicated [211] direction.

These studies suggest that the stepped structure of the Cu(211) surface does not significantly perturb its bulklike electronic structure, a result which was anticipated in previous work.^{20,45} In contrast to this, it would be interesting to investigate the valence-band-structure properties of stepped crystal faces of the catalytically active group-VIII metals, particularly in light of recent Pt(100)-(5 \times 1) results,¹⁴ which showed large DOS contributions to the normal-emission EDC's for the reconstructed surface.

Based on these Cu(211) results, we conclude that bulk valence-band-structure determination can be applied to low-symmetry directions in a manner analogous to the (111), (100), and (110) faces, thereby alleviating the necessity for crystal faces with a specific high-symmetry orientation. This has implications for band-structure studies of more complicated materials, where it may not be possible to obtain high-symmetry faces.

Finally, we summarize the major results of this work: (1) It is possible to determine experimental valence-band dispersion relations for non-low-index directions; (2) valence-band dispersion relations for stepped Cu(211) show excellent agreement with bulk valence bands interpolated along the [211] direction; and (3) the quasi-free-electron model describes photoelectron dispersion relations satisfactorily for photoemission from Cu(211).

ACKNOWLEDGMENTS

We wish to thank K. A. Mills and J. G. Tobin for assistance in carrying out some of the photoemission measurements, and Mrs. Winifred Heppler for assisting in the

preparation of the copper crystal. In addition, we acknowledge M. G. Mason for many stimulating discussions. This work was supported by the Director, Office of Energy Research, Office of Basic Energy Sciences, Chemical Sciences Division of the U. S. Department of Energy,

under Contract No. DE-AC03-76SF00098. It was performed at the Stanford Synchrotron Radiation Laboratory, which is supported by the Department of Energy, Office of Basic Energy Sciences and the National Science Foundation, Division of Materials Research.

*Present address: Polaroid Corporation, Waltham, MA 02154.

†Present address: Department of Chemistry and Biochemistry, University of California, Los Angeles, CA 90024.

‡Present address: AT&T Bell Laboratories, Murray Hill, NJ 07974.

§Present address: Tennessee Eastman Company, Kingsport, TN 37662.

¹J. Stöhr, P. S. Wehner, R. S. Williams, G. Apai, and D. A. Shirley, *Phys. Rev. B* **17**, 587 (1978); D. A. Shirley, J. Stöhr, P. S. Wehner, R. S. Williams, and G. Apai, *Phys. Scr.* **16**, 398 (1977).

²J. A. Knapp, F. J. Himpsel, and D. E. Eastman, *Phys. Rev. B* **19**, 4952 (1979).

³P. O. Nilsson and L. Ilver, *Solid State Commun.* **17**, 667 (1975); L. Ilver and P. O. Nilsson, *ibid.* **18**, 677 (1976).

⁴P. Thiry, D. Chandris, J. Lecante, C. Guillot, R. Pinchaux, and Y. Petroff, *Phys. Rev. Lett.* **43**, 82 (1979).

⁵Z. Hussain, S. Kono, L.-G. Petersson, C. S. Fadley, and L. F. Wagner, *Phys. Rev. B* **23**, 724 (1981), and references therein.

⁶P. S. Wehner, R. S. Williams, S. D. Kevan, D. Denley, and D. A. Shirley, *Phys. Rev. B* **19**, 6164 (1979), and references therein.

⁷G. V. Hansson and S. A. Flodström, *Phys. Rev. B* **17**, 473 (1978).

⁸K. A. Mills, R. F. Davis, S. D. Kevan, G. Thornton, and D. A. Shirley, *Phys. Rev. B* **22**, 581 (1980).

⁹A. E. Schach von Wittenau, R. F. Davis, J. G. Tobin, M. G. Mason, Z. Hussain, and D. A. Shirley (unpublished).

¹⁰P. Heimann, H. Miosga, and H. Neddermeyer, *Solid State Commun.* **29**, 463 (1979).

¹¹G. V. Hansson and S. A. Flodström, *Phys. Rev. B* **18**, 1572 (1978).

¹²D. E. Eastman, F. J. Himpsel, and J. A. Knapp, *Phys. Rev. Lett.* **40**, 1514 (1978); F. J. Himpsel, J. A. Knapp, and D. E. Eastman, *Phys. Rev. B* **19**, 2919 (1979).

¹³F. J. Himpsel and D. E. Eastman, *Phys. Rev. B* **18**, 5236 (1978).

¹⁴G. Thornton, R. F. Davis, K. A. Mills, and D. A. Shirley, *Solid State Commun.* **34**, 87 (1980).

¹⁵J. F. van der Veen, F. J. Himpsel, and D. E. Eastman, *Phys. Rev. B* **22**, 4226 (1980).

¹⁶R. F. Davis, K. A. Mills, G. Thornton, S. D. Kevan, and D. A. Shirley, Proceedings of the VIth International Conference on Vacuum Ultraviolet Radiation Physics, Extended Abstracts, University of Virginia, Charlottesville, Virginia, 1980 (unpublished).

¹⁷B. Feuerbacher and R. F. Willis, *J. Phys. C* **9**, 169 (1976).

¹⁸See, e.g., Gabor A. Somorjai, *Chemistry in Two Dimensions: Surfaces* (Cornell University Press, Ithaca, New York, 1981), Chap. 4.

¹⁹G. A. Somorjai, *Adv. Catal.* **26**, 1 (1977); D. W. Blakely and G. A. Somorjai, *J. Catal.* **42**, 181 (1976).

²⁰R. S. Williams, P. S. Wehner, S. D. Kevan, R. F. Davis, and D. A. Shirley, *Phys. Rev. Lett.* **41**, 323 (1978).

²¹K. Ždánký and Z. Šroubek, *J. Phys. F* **6**, L205 (1976).

²²M. C. Desjonquères and F. Cyrot-Lackmann, *Solid State Commun.* **18**, 1127 (1976).

²³Y. W. Tsang and L. M. Falicov, *J. Phys. C* **9**, 51 (1976).

²⁴We used a solution of sodium 2-mercaptobenzimidazole-5-sulfonate and polyethylene glycol 400 in HCl; see J. S. Ahearn, J. P. Monaghan, and J. W. Mitchell, *Rev. Sci. Instrum.* **41**, 1853 (1970).

²⁵B. Lang, R. Joyner, and G. A. Somorjai, *Surf. Sci.* **30**, 440 (1972); **30**, 454 (1972).

²⁶S. D. Kevan and D. A. Shirley, *Phys. Rev. B* **22**, 542 (1980).

²⁷G. D. Mahan, *Phys. Rev. B* **2**, 4334 (1970).

²⁸Peter J. Feibelman and D. E. Eastman, *Phys. Rev. B* **10**, 4932 (1974); F. J. Himpsel, *Appl. Opt.* **19**, 3964 (1980).

²⁹See, e.g., R. S. Williams, P. S. Wehner, J. Stöhr, and D. A. Shirley, *Surf. Sci.* **75**, 215 (1978); also see Refs. 1, 6, 8, 9, 14, and 16.

³⁰The *d*-band interpolation scheme of N. V. Smith has been described and applied in a series of publications. Those most relevant to this paper are N. V. Smith and L. F. Mattheiss, *Phys. Rev. B* **9**, 1341 (1974); N. V. Smith, *ibid.* **19**, 5019 (1979).

³¹L. Hodges, H. Ehrenreich, and N. D. Lang, *Phys. Rev.* **152**, 505 (1966).

³²J. F. Janak, A. R. Williams, and V. L. Moruzzi, *Phys. Rev. B* **11**, 1522 (1975).

³³Glenn A. Burdick, *Phys. Rev.* **129**, 138 (1963).

³⁴E. Dietz and F. J. Himpsel, *Solid State Commun.* **30**, 235 (1979).

³⁵J. Hermanson, *Solid State Commun.* **22**, 9 (1977).

³⁶F. J. Himpsel, *Appl. Opt.* **19**, 3964 (1980), and references therein.

³⁷P. O. Gartland, S. Berge, and B. J. Slagsvold, *Phys. Norv.* **7**, 39 (1973).

³⁸S. Andersson, *Surf. Sci.* **18**, 325 (1969).

³⁹M. R. Halse, *Philos. Trans. R. Soc. London, Ser. A* **265**, 507 (1969).

⁴⁰J. A. Stratton, *Electromagnetic Theory* (McGraw-Hill, New York, 1941), Chap. IX.

⁴¹N. V. Smith, R. L. Benbow, and Z. Hurych, *Phys. Rev. B* **21**, 4331 (1980).

⁴²J. B. Pendry, *Surf. Sci.* **57**, 679 (1979); *Low Energy Electron Diffraction* (Academic, New York, 1974).

⁴³P. O. Nilsson and N. Dahlbäck, *Solid State Commun.* **29**, 303 (1979).

⁴⁴P. O. Nilsson, J. Kanski, and C. G. Larsson, *Solid State Commun.* **36**, 111 (1980).

⁴⁵G. S. Painter, P. J. Hennings, and R. O. Jones, *J. Phys. C* **8**, L199 (1975).